Corrosion Science 50 (2008) 3371–3377

Contents lists available at ScienceDirect

Corrosion Science

journal homepage: www.elsevier.com/locate/corsci

Microstructural effects on the hydrogen permeation of an Inconel alloy 690

J.M. Zagal [a,c], H.F. López [b,*], O. Flores [a], J.L. Albarran [a], L. Martínez [a]

[a] Centro de Ciencias Físicas, UNAM, P.O. Box 48-3, C.P. 62251, Cuernavaca, Morelos, Mexico
[b] Materials Department, University of Wisconsin – Milwaukee, P.O. Box 784, Milwaukee, WI 53201, USA
[c] Facultad de Química, UNAM, Ciudad Universitaria, C.P. 04510, Mexico

ARTICLE INFO

Article history:
Received 28 February 2008
Accepted 22 August 2008
Available online 2 September 2008

Keywords:
A. Nickel
B. Hydrogen permeation
C. Kinetic parameters
C. Stress corrosion

ABSTRACT

In the present work, hydrogen permeability tests were carried out in Inconel 690 in the as-received (AR) condition and after heat treating. The heat treatments promoted total solid solution (SA) or a microstructure full of grain boundary (gb) coverage with $M_{23}C_6$ carbides (A800). first and second polarization hydrogen transients were determined and used in disclosing the role of reversible and irreversible hydrogen trapping. It was found that in the SA condition, the permeation rates were the highest but they were significantly reduced in the AR condition, particularly in the A800 due to the presence of gb $M_{23}C_6$ carbides.
Published by Elsevier Ltd.

1. Introduction

Inconel alloy 690 which contains ~28 to 30 wt. pct. Cr (twice the Cr found in Inconel 600) has been found to exhibit superior stress corrosion cracking (SCC) resistance when exposed to pressurized water reactor (PWR) environments as compared with Inconel alloy 600 [1–8]. Accordingly, this alloy is currently being used or considered in replacing components made of alloy 600. Thus far, there are no reports of SCC failures in components made of alloy 690 exposed to PWR environments. In contrast, alloy 600 has been found to be susceptible to intergranular stress corrosion cracking (IGSCC) under PWR operating conditions, with the effect being exacerbated when the alloy is in the solid solution condition [9–15]. Moreover, the severity of IGSCC is significantly enhanced when hydrogen evolution (i.e., under cathodic conditions) is prevalent in the environment [9,12].

Since hydrogen evolution is generated or involved during crack initiation/growth in Inconel alloys exposed to PWR environments, it is essential to disclose the role of hydrogen in these environments. Extensive experimental evidence indicates that under these conditions, there is a build up of elevated hydrogen concentrations in Ni-based alloys [9,16], well beyond those predicted by Sieverts's law (upto 20–80 ppm atomic hydrogen [16]). In turn, this suggests the presence of appreciable hydrogen trapping sites which are expected to play a key role on the effective hydrogen diffusivity and potential alloy susceptibility to hydrogen embrittlement.

Among the published works on hydrogen permeation in Inconel 690, Symons et al. [16] found two hydrogen desorption peaks corresponding to reversible and irreversible hydrogen trapping. In their work, they estimated trapping binding energies, E_b of 37 kJ/mol for irreversible carbide traps of the $M_{23}C_6$ type. Moreover, they found that plastic straining influences E_b to some extent. In the case of irreversible traps, they found that the E_b associated with gb $M_{23}C_6$-matrix interfaces increased from 37 kJ/mol at 0 pct. strain to 41 kJ/mol at 10 pct. plastic strain.

To date there is still not enough evidence available in the literature on Inconel alloy 690 to conclusively affirm that this alloy is immune to IGSCC. From the published literature [7], it is apparent that once a crack is initiated by mechanical means, crack propagation apparently occurs in this alloy under PWR environments. Moreover, Sui et al.'s [8] have found that alloy 690 can develop intergranular cracks in U-bend specimens exposed to hydrogen-steam conditions. Hence, it is important to establish the interaction between any absorbed atomic hydrogen and the alloy microstructure including plastic straining effects. In this work, the hydrogen permeability properties of Inconel alloy 690 under various heat conditions were investigated. In particular, the apparent hydrogen diffusivities were linked to possible trapping effects associated with the exhibited microstructures.

2. Experimental

The Inconel alloy 690 in the as-received condition (AR) was provided by Allvac Corporation as a one inch thick plate stock in a mill annealed condition. The grain structure was equiaxed with an average grain size of 29.6 μm. Table 1 shows the composition of

* Corresponding author. Tel.: +1 414 229 6005; fax: +1 414 229 6958.
E-mail address: Lopez@uwm.edu (H.F. López).

0010-938X/$ - see front matter Published by Elsevier Ltd.
doi:10.1016/j.corsci.2008.08.042

Table 1
Chemical composition of Inconel Alloy 690 (wt.%)

Ni	Cr	Fe	Mn	Si	Cu	Ti	C
61.66	27.52	9.21	0.19	0.50	0.50	0.37	0.05

the Inconel 690 alloy used in this work. Inconel alloy bars were cut from this plate and heat treated at 1150 °C for 15 min (solid solution anneal, SA) followed by oil cooling. In addition, various SA alloy bars were subsequently annealed at 800 °C for 1 h and then oil cooled (A800). Table 2 gives the exhibited mechanical properties of the Inconel alloy in the as-received and heat treated conditions.

Microstructural characterization of the Inconel alloy 690 samples (AR, SA and A800) was made by metallographic means followed by electrolytical etching in a 6% nital solution under 4 V for 3 min. Optical and scanning electron microscopy (SEM) including EDS were used for microstructural determinations. Fig. 1 shows the geometry and dimensions of the machined Inconel alloys used as electrochemical permeability membranes in this work. These membranes were prepared by electrical discharge machining all the way down to 500 μm thickness. Final preparation of the membrane surfaces was attained by surface grinding and polishing all the way to mirror finishing.

2.1. Hydrogen permeation testing

Hydrogen permeation was electrochemically measured using two cells separated by the Inconel 690 membrane. The technique proposed by Devanathan and Stachurski [17] (G 148-97 standard) was used in this work. Fig. 2 shows schematically the electrochemical system employed for permeability testing. The electrolyte in the loading cell (cathodic side) consisted of 0.1 mol/l H_2SO_4 with 5×10^{-5} mol/l As_2O_3, whereas the oxidation cell side was under a 0.1 N NaOH solution. The membrane area exposed to the electrolyte solutions was 2.230 cm^2.

Table 2
Exhibited mechanical properties of Inconel 690 as a function of the heat condition

Material condition	UTS (MPa)	σ_y (MPa)	σ_{fract} (MPa)	Elongation (%)	Reduction in area (%)
As-received	552	168	364	52.2	58.4
Solid solution	504	132	225	64.9	69.0
800 anneal	497	126	362	61.0	49.3

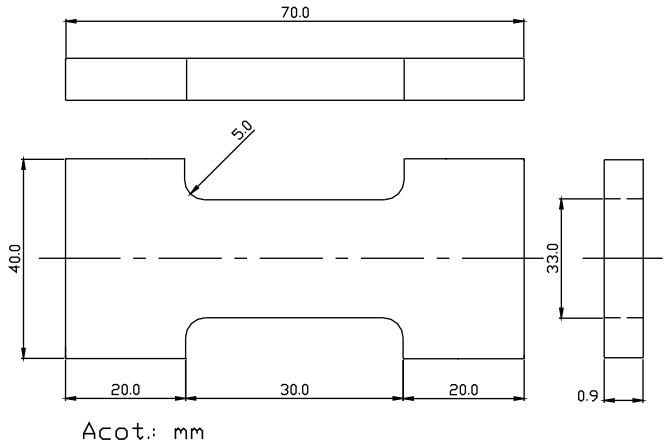

Fig. 1. Geometry and dimensions of Inconel 690 hydrogen membranes.

Prior to running any permeability tests, the electrolyte solutions were bubbled with nitrogen for approximately 2 h. A saturated Calomel reference electrode (SCE) and a graphite auxiliary electrode were placed in the oxidation cell (anode), including a nitrogen bubbling system. Both cell compartments were deoxygenated by bubbling nitrogen through the electrolyte solutions before and during testing. The electrochemical system was a 953 ACM Gill-AC computer driven potentiostat, which included a precise thermostatic temperature control at 25 °C ± 0.1. An oxidation potential of +300 mV versus the SCE electrode was established for hydrogen oxidation. Once a static passive state was reached in the oxidation cell, the 0.1 mol / l H_2SO_4 with 5×10^{-5} mol / l As_2O_3 electrolyte solution was introduced in the cathodic cell side and immediately polarized with a cathodic current of 10 mA/cm^2. The temperature of the system was adjusted and the system pressurized to follow the hydrogen permeation current as a function of time until steady state was reached. In addition, transient hydrogen flow was monitored through measurements of current permeability transients.

3. Results and discussion

3.1. Exhibited microstructures

The microstructures of the as-received and heat treated inconel alloy 690 are shown in Fig. 3. Notice that the grain structure is somewhat inhomogeneous as there are regions consisting of small and large grains. In addition, there are some twins and significant discrete grain boundary (gb) carbide coverage in the AR condition (Fig 3a). The present carbide phases were identified by electron diffraction as $M_{23}C_6$ and they were preferentially found along the gbs. In the SA condition, $M_{23}C_6$ gb carbides were almost totally dissolved resulting in essentially carbide-free gb structures (Fig. 3b).

Heat treating at 800 °C for 1 h lead to copious gb precipitation of semi-continuous carbide films some of them of the dendrite/globular type [3,16] as shown in Fig. 3c. In addition, relatively coarse Ti containing phases were found to be present both, at the gbs and within the bulk (Fig. 3d). Fig 4a and b shows a coarse Ti-particle and corresponding EDS peaks in a fractured Inconel membrane. Notice that Ti is the main element in this precipitate. In addition, elemental composition mapping using EDS of the Ti-particles further confirmed that Ti is the main element (Fig. 5a–d). Apparently, these Ti-phases developed during alloy processing as heat treating did not promote any significant dissolution nor coarsening. From the published literature, it is apparent that these phases are Ti-nitrides and not Ti-carbonitrides as suggested by Venkatesh et al., [18] and as evidenced by the observations of this work of a lack of carbon in these phases (see Fig. 5). Table 3 gives the mean precipitate size as well as the estimated precipitate densities found for each of the heat conditions.

3.2. Permeability

Fig. 6a shows first polarization hydrogen transients for the as received and heat treated membranes obtained under identical electrochemical testing conditions. First permeation transients yield information on the concurrent behavior of reversible and irreversible trapping sites. Notice from these polarization curves that hydrogen transport in the SA condition is relatively fast when compared with either the AR or the A800 conditions. Apparently, in the SA condition, steady state is reached earlier than in any other heat conditions due to the lack of gb $M_{23}C_6$ carbides which are expected to act as effective irreversible hydrogen trapping sites [16].

The resultant steady state permeation fluxes (J_{ss}), as well as effective hydrogen diffusivities (D_{eff}) and hydrogen surface concentrations (C_o) were estimated by considering the widely employed